Carbon 203 (2023) 1–10

Contents lists available at ScienceDirect

Carbon

journal homepage: www.elsevier.com/locate/carbon

Rational synthesis of silane-functionalized carbon dots with high-efficiency full-color solid-state fluorescence for light emitting diodes

Guangzhou Hu [a], Yang Wang [a], Shuang Zhang [a], Hui Ding [a,*], Ziyuan Zhou [b], Jishi Wei [c], Xuehua Li [a], Huanming Xiong [c,**]

[a] Key Laboratory of Coal Processing and Efficient Utilization of Ministry of Education and College of Chemical Engineering, China University of Mining and Technology, Xuzhou, 221116, Jiangsu, PR China
[b] National Cancer Center/National Clinical Research Center for Cancer/Cancer Hospital & Shenzhen Hospital, Chinese Academy of Medical Sciences and Peking Union Medical College, Shenzhen, 518116, PR China
[c] Department of Chemistry, Shanghai Key Laboratory of Molecular Catalysis and Innovative Materials, Fudan University, Shanghai, 200433, PR China

ARTICLE INFO

Keywords:
Carbon dots
Solid-state fluorescence
Tunable full-color emission
Emission mechanism
Light-emitting diodes

ABSTRACT

Highly efficient full-color solid-state fluorescent carbon dots (CDs) are very critical for the construction of light-emitting diodes (LEDs), especially white light-emitting diodes (WLEDs), but achieving them is still a challenging task due to the serious self-quenching of CDs in the aggregation state and their complicated photoluminescence (PL) mechanism. Herein, we reported a one-step microwave-assisted method for the large-scale synthesis of solid-state silane-functionalized CDs (SiCDs) with self-quenching resistant and tunable full-color fluorescence. By only controlling the ratio of precursors, the PL emission of these SiCDs can be tuned in the visible region ranging from 438 to 633 nm, accompanied by high quantum yields (QYs) of up to 26-57%. The multicolor emission of these SiCDs is ascribed to their differences in particle size and graphitic nitrogen content, which can be modulated by controlling the dehydration and condensation reactions among raw materials. In addition, based on their excellent optical properties, these SiCDs were directly utilized as phosphors combing with ultraviolet chips to prepare full-color LEDs and all types of WLEDs with adjustable correlated color temperature (CCT) from 3678 to 8158 K and high color rendering index (CRI) of 90–94, demonstrating the tremendous potential for practical lighting applications.

1. Introduction

As newly-emerging luminescent nanomaterials, multicolor emissive carbon dots (CDs) have received increasing attention owing to their intrinsic merits of controllable photoluminescence (PL), high stability, outstanding biocompatibility, and low cost [1–6]. By far, remarkable progress has been achieved in the design and synthesis of CDs with efficient multicolor emission in solutions [7–9]. However, once in a solid or powder state, most CDs are self-quenched due to excessive fluorescence resonance energy transfer (FRET) or direct $\pi-\pi$ interaction, making the obtained CD powders with weak or no fluorescence, thereby substantially limiting their direct use as phosphors for fabricating light-emitting diodes (LEDs) [10–12]. To preserve the multicolor fluorescence of CDs in the solid state, the commonly used method is to disperse them into inert solid matrices, such as polymer, starch, sodium silicate, inorganic salt, and so on [13–19]. Nevertheless, the obtained CD composites still suffer from serious aggregation-induced PL quenching (AIQ) because the structural compositions of CDs are not altered in essence. In this case, the loading fraction of CDs in matrices is always rather low, and the fluorescence is identical to that of dilute CD solution, which fails to provide sufficient PL output or adjust emission color for high-performance photoelectric devices [20–22]. At the same time, these mixing methods are usually accompanied by other disadvantages, such as uneven dispersion, poor stability, low production yield, multi-step procedures, and tedious reaction time, which are very unfavorable for the industrial production and practical applications of solid-state fluorescent CDs [23–25]. Thus, it is urgent and necessary to develop a fast, and one-step method for producing self-quenching-resistant solid-state CDs with high-efficiency multicolor emission on a large scale.

---

* Corresponding author.
** Corresponding author.
E-mail addresses: hding@cumt.edu.cn (H. Ding), hmxiong@fudan.edu.cn (H. Xiong).

https://doi.org/10.1016/j.carbon.2022.11.048
Received 12 August 2022; Received in revised form 31 October 2022; Accepted 18 November 2022

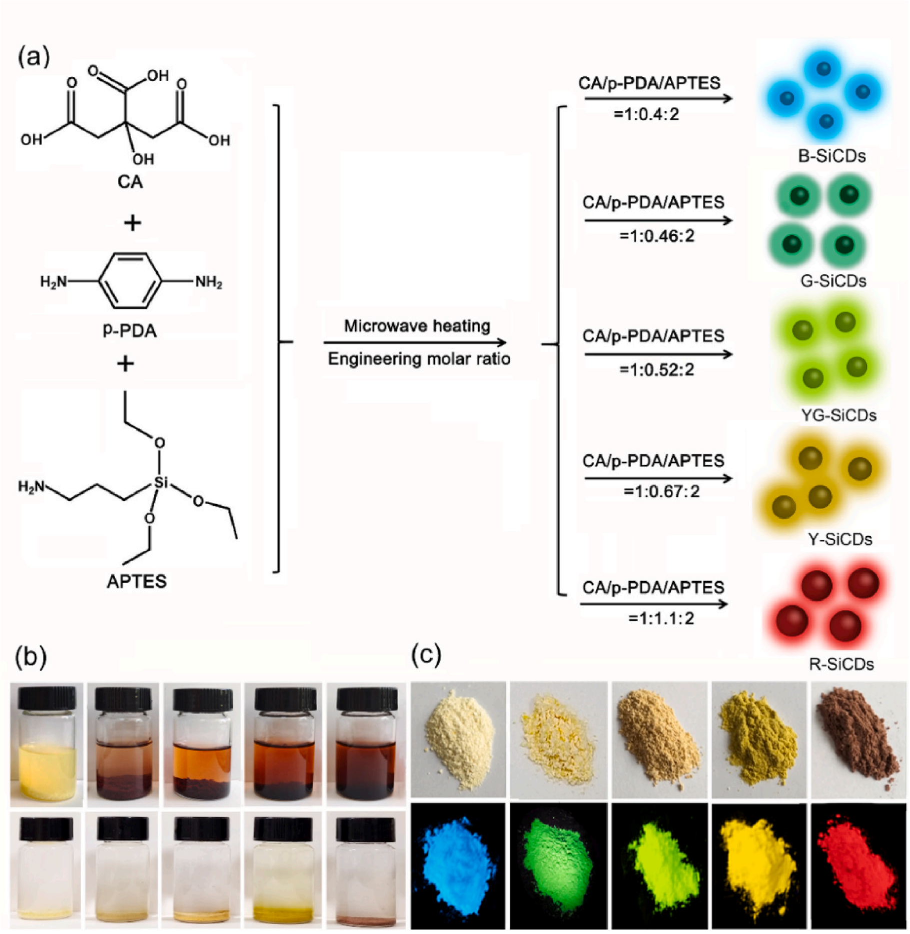

Fig. 1. (a) Schematic diagram of the preparation of SiCDs with full-color solid-state fluorescence. Optical images of SiCDs synthesized with different molar ratios of CA/p-PDA/APTES: (b) initial solutions before (up) and after (below) centrifugation, and (c) collected powders under visible light (up) and under 365 nm UV light (below). (A colour version of this figure can be viewed online.)

To this end, the underlying PL mechanism of CDs in the solid state should be deeply explored, which involves self-quenching resistance, emission color tuning, and quantum yield (QY) enhancement [18,26,27]. In recent years, a few research groups have produced matrix-free CDs with intense solid-state luminescence from various raw materials and tried to clarify the intrinsic relationship between the solid-state PL performances of CDs and their structural compositions. For example, Chen et al. prepared yellow emissive CD powders from poly(vinyl alcohol) (PVA) and ethylenediamine (EDA), and found that the PVA chains on the CD surfaces can segregate CDs to realize solid-state luminescence [28]. Zhu et al. produced CDs with tunable solid-state emission from 425 to 580 nm using polyvinylpyrrolidone (PVP) and urea as precursors, where the increment in the particle size and nitrogen content collaboratively resulted in a red shift in emission wavelength [29]. Wang et al. synthesized orange-emissive CDs with a solid-state QY of 39% through heating an aqueous solution of phloroglucinol, ethylenediamine, and boric acid, whose strong luminescence was ascribed to a high content of graphitic nitrogen in the obtained CDs [23]. These preliminary works demonstrate that the solid-state PL performances of CDs can be modulated by synergistically controlling their chemical structures. Accordingly, if choosing suitable organic molecules as carbon sources, rationally regulating the dehydration and carbonization reactions between them would be a feasible strategy to produce self-quenching resistant CDs with desired solid-state luminescence. To the best of our knowledge, however, no report has been reported so far regarding the preparation of CDs with bright full-color solid-state luminescence by regulating their growth processes in a single reaction system.

In this study, we report a fast, and one-step microwave-assisted route to acquire solid-state SiCDs with highly efficient full-color emission using citric acid (CA), p-phenylenediamine (p-PDA), and (3-aminopropyl) triethoxysilane (APTES) as raw materials. Thereinto, the APTES can serve not only as the carbon sources of CDs but also as the surface passivation agents to inhibit the AIQ effect. Just by adjusting the p-PDA amount in reactions, the particle size and graphitic nitrogen content of SiCDs are modulated over a wide range, both of which trigger the observed PL red shift from 438 to 633 nm, covering the entire visible spectrum. This is the first time to realize the synthesis of tunable full-color solid-state fluorescent CDs by using the single factor variable method. In addition, these solid-state SiCDs have a high PLQY of up to 57%, a high production yield of up to 84%, and excellent photostability. Finally, these phosphors are combined with an ultraviolet (UV) chip to fabricate multicolor light-emitting diodes (LEDs), and all types of white LEDs (WLEDs), including warm-WLEDs, standard-WLEDs, and cool-WLEDs.

2. Experimental section

2.1. Materials

Citric acid (CA), p-phenylenediamine (p-PDA), and (3-aminopropyl) triethoxysilane (APTES), ethanol, and polyvinyl alcohol (MW = 96,500) were purchased from Shanghai Maclin Biochemical Technology Co., LTD. Ethanol was obtained from Xilong Scientific Co., Ltd. GaN LEDs

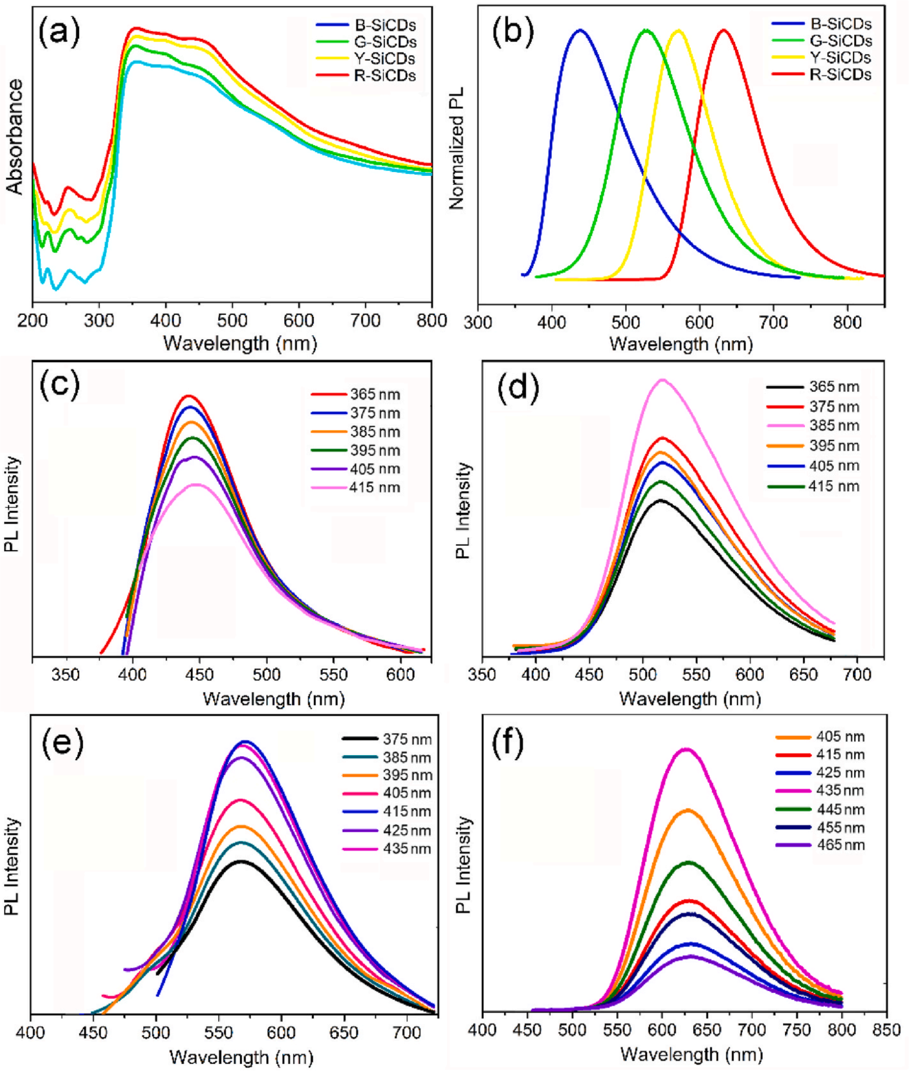

Fig. 2. (a) The absorption spectra and (b) normalized PL emission spectra of the four selected SiCDs. PL spectra of (c) B-SiCDs, (d) G-SiCDs, (e) Y-SiCDs, and (f) R-SiCDs excited by different wavelengths of light. (A colour version of this figure can be viewed online.)

chips without phosphor coating were offered from Shenzhen Zhanlong Technology Co., LTD. Ultrapure (Milli-Q) water was made in the laboratory. All the chemicals were analytical grade and used as received without further purification.

2.2. *Characterizations*

The morphologies of SiCDs were observed by a MAIA3 LMH scanning electron microscope. Transmission electron microscope (TEM) and high-resolution TEM (HRTEM) images were collected on an FEI-Tecnai G2 transmission electron microscope at an acceleration voltage of 200 kV. Ultraviolet–visible (UV–vis) absorption spectra were obtained on a Shimadzu UV-3101 PC spectrophotometer. PL spectra of SiCDs were measured on an F-4600 Hitachi fluorescence spectrometer. Fourier-transform infrared (FTIR) spectra were recognized using a Magna IR-560 FTIR spectrometer. Raman spectra were gathered with an XploRA Raman spectrometer under 785 nm of laser irradiation. X-ray photoelectron spectra were measured with an AXIS Ultra DLD spectrometer. Time-resolved fluorospectroscopy was detected using an FLS 920 spectrometer. Photographs of SiCDs powders were taken with a camera (Canon EOS 800D) at an excitation wavelength of 365 nm. The emission spectra, Commission Internationale de L'Eclairage (CIE) coordinates, color rendering index (CRI), and correlated color temperature (CCT) of LEDs were measured on a HAAS-2000 spectroradiometer.

2.3. *Synthesis of SiCDs with full-color emission*

These SiCDs with tunable solid-state emissions from blue to red were produced from CA, p-PDA, and APTES via a one-step microwave-assisted method. In detail, 0.48 g of CA (2.5 mmol), 0.11 g of p-PDA (1 mmol), and 1.12 g of APTES (5 mmol) were added to 30 mL of ethanol aqueous solution (the volume ratio between ethanol and water is 1:1), and sonicated at room temperature for 5 min then heated at 400 W for 10 min in a domestic microwave oven (MDS-6G). After the reaction, the resulting precipitates were collected by centrifugation at 3000 rpm for 10 min, followed by washing with a mixed solution of ethanol and water (volume ratio of 2:1) by four times, and finally dried in a vacuum oven at 40 °C overnight to obtain the blue-emitting SiCD powders. For other samples, their preparation processes were almost the same as above except that the amount of p-PDA added was changed to 0.12, 0.14, 0.18, and 0.30 g for green, greenish-yellow, yellow, and red emission SiCDs, respectively.

2.4. *Fabrication of multicolor and white LEDs*

Commercially available UV chips (365 nm) with an operating

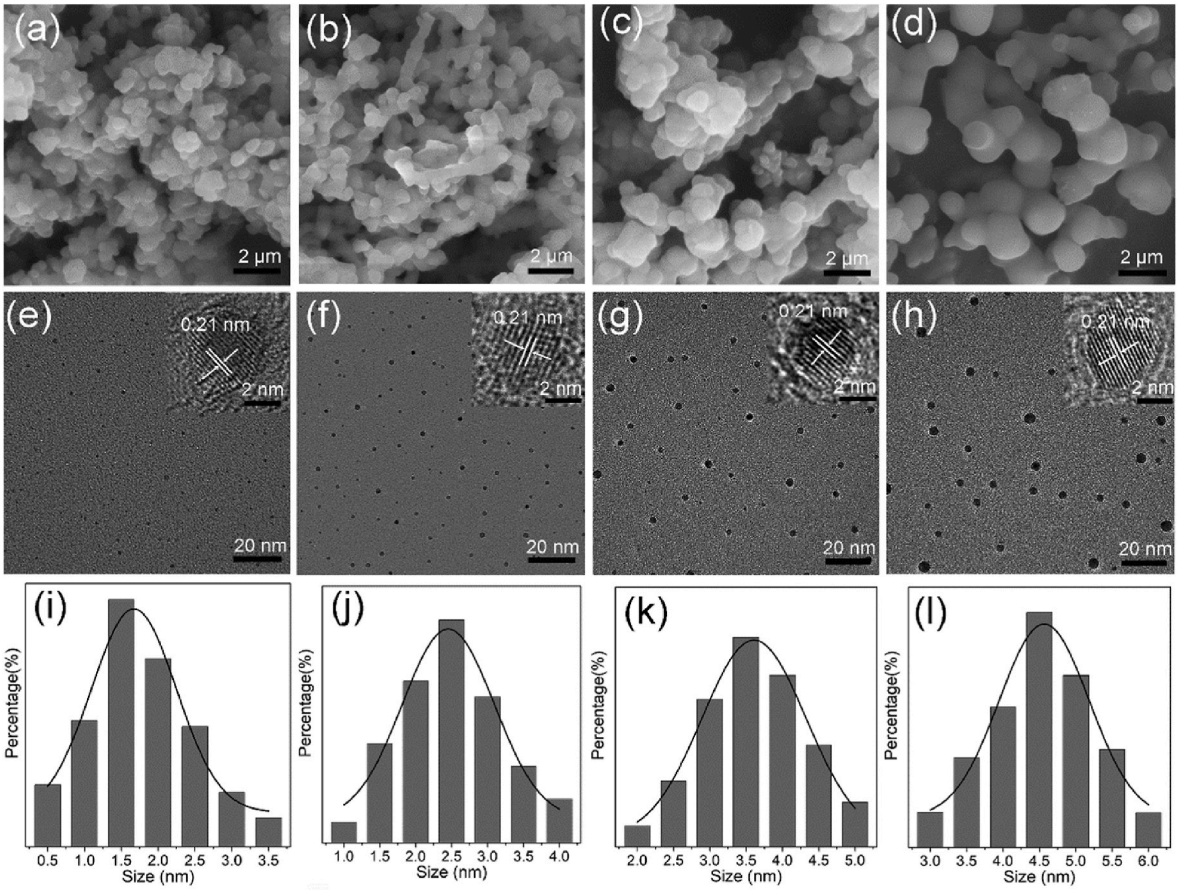

Fig. 3. SEM images of (a) B-SiCDs, (b) G-SiCDs, (c) Y-SiCDs, and (d) R-SiCDs. TEM and HRTEM images (inset) of (e) B-SiCDs, (f) G-SiCDs, (g) Y-SiCDs, and (h) R-SiCDs. Particle size distribution diagrams of (i) B-SiCDs, (j) G-SiCDs, (k) Y-SiCDs, and (l) R-SiCDs. (A colour version of this figure can be viewed online.)

voltage of 4.0 V were used as an excitation source for fabricating all types of LEDs. Specifically, 0.1 g of B-, G-, Y-, and R-SiCDs powders were mixed, respectively, in a total volume of 10 mL of silicone resin. Subsequently, the mixed colloid was thoroughly stirred until homogeneous, coated on the surface of a GaN UV-LED chip, and then dried in an oven for 1 h at 100 °C. Finally, the multicolor LEDs were obtained. Similar procedures were followed to fabricate the white LEDs only with different weight ratios of B-SiCDs, G-SiCDs, and R-SiCDs dispersed in silicone resin.

3. Results and discussion

These SiCDs with tunable full-color solid-state fluorescence were synthesized from CA, p-PDA, and APTES by a facile one-step microwave-assisted heating method (Fig. 1a). These precursors are carefully selected because each one is essential for the successful production of SiCDs. For example, when the reaction proceeded without adding CA or APTES, the obtained two kinds of CDs emit strong yellow and blue luminescence in the solution state, respectively, indicating that the addition of p-PDA can result in red-shifting the emission of CDs (Fig. S1) [30]. However, the corresponding CD powders are self-quenched under UV light (Fig. S3), which is contrary to the CDs synthesized in the absence of p-PDA (Fig. S2), suggesting that CA and APTES are crucial to inhibiting the AIQ effect [31]. The results of control experiments demonstrate that CA, p-PDA, and APTES work together to produce the final SiCDs with tunable solid-state luminescence. By controlling the molar ratio of CA/p-PDA/APTES to 1:0.4:2, 1:0.46:2, 1:0.52:2, 1:0.67:2, and 1:1.1:2, five powdered SiCDs emitting blue, green, yellowish-green, yellow, and red fluorescence, were obtained, which are named B-SiCDs, G-SiCDs, YG-SiCDs, Y-SiCDs, and R-SiCDs, respectively. These SiCD powders show a dramatic color change from light-yellow to brown in the daylight (Fig. 1c, top) and red-shifted fluorescence colors from blue to red under a UV light of 365 nm (Fig. 1c, down). It should be noted that the resulting SiCDs were insoluble in this ethanol-water reaction medium with a volume ratio of 1:1, and could be easily collected as a powder after centrifugation (Fig. 1b). With respect to the feeding mass of raw materials, the production yields of the obtained samples are calculated to be 68%, 84%, 79%, 76%, and 80% for B-, G-, YG-, Y-, and R-SiCDs, respectively, providing a promising possibility for their industrial-scale production. To understand the effect of reaction conditions on the PL emission and structural compositions of these SiCDs, four types of powdered SiCDs, including B-, G-, Y-, and R-SiCDs, are selected as model samples for further characterizations.

The ultraviolet–visible (UV/Vis) absorption spectra of the four SiCDs are shown in Fig. 2a. Different from CDs in the solution state [32–34], our powdered SiCDs present weak absorption in the UV region but strong absorption in the visible region, which may be related to the abundant silicon chains on the surface of CDs [20]. In the UV region, two distinct absorption peaks appear at 225 and 258 nm, which are attributed to the π–π* transitions of C=C and C=N bonds in carbon cores, respectively [35]. However, in the visible region, the four SiCDs exhibit distinct absorption bands at about 380, 396, 426, and 435 nm, respectively, which are assigned to the n–π* transitions of C–N/C=N or C–O/C=O bonds on the surface of SiCDs [30]. The PL spectra of the four samples in Fig. 2c–f demonstrate an excitation-independent behavior with peaks at 438, 514, 577, and 633 nm for B-SiCDs, G-SiCDs, Y-SiCDs, and R-SiCDs, respectively [36]. The PL excitation spectra of these SiCDs are observed to be well overlapped with their corresponding absorption bands in the visible region (Fig. S4), indicating that the blue, green, yellow, and red-light emissions originate from their different

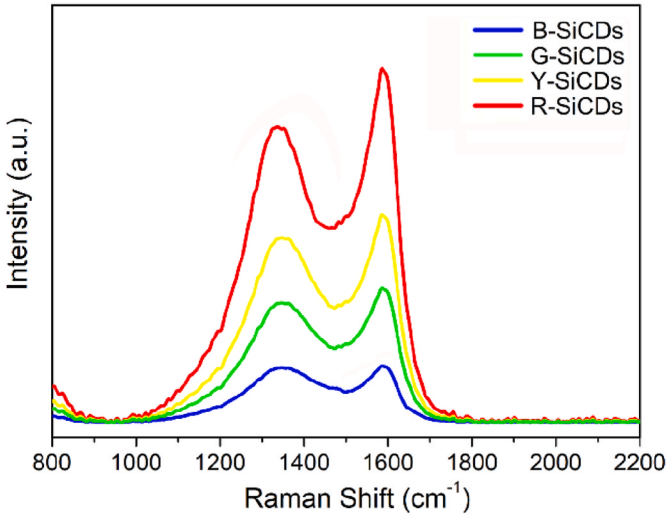

Fig. 4. Raman spectra of the four selected SiCDs. (A colour version of this figure can be viewed online.)

luminescent centers [37]. Under their optimal excitation wavelengths, the absolute fluorescent QYs of B-SiCDs, G-SiCDs, Y-SiCDs, and R-SiCDs measured by an integrating sphere are determined to be 41%, 33%, 57%, and 26%, respectively, which are much higher than those of other previously reported multicolor solid CDs (Table S1). Furthermore, the optical properties of each sample were further investigated by the time-resolved PL decay spectra. The results in Fig. S5 and Table S2 show that the PL decays of the four samples are well fitted by a double-exponential function, comprising a fast component of τ_1 (1.0 ns) and a slow component of τ_2 (7.0 ns), which are corresponding to the recombination pathways of the core states and surface states, respectively [33]. It is not difficult to see that from B-SiCDs to R-SiCDs, as the average lifetime decreases from 4.33 to 3.04 ns, the τ_1 weight increases from 37.13 to 64.63%, indicating that the radiative recombination of the core states dominantly contributes to the PL red shift of these SiCDs [35]. The above data demonstrate that these SiCDs we present here possess favorable and uniform solid-state fluorescence properties and their multicolor emission result from the change of carbon cores regulated by the different mole ratios of p-PDA in reactants.

The morphologies and sizes of the four typical SiCDs were observed by scanning electron microscope (SEM) and transmission electron microscopy (TEM). As shown in Fig. 3a–d, the SEM images exhibit that the four SiCDs are all uniform quasi-spherical particles with irregular aggregation. The TEM images presented in Fig. 3e–h illustrate that these particles are evenly distributed nanodots with a rather broad size distribution (Fig. 3i–l). By counting more than 100 particles, the average lateral sizes of B-SiCDs, G-SiCDs, Y-SiCDs, and R-SiCDs are estimated to be approximately 1.6, 2.7, 3.5, and 4.6 nm, respectively, indicating that the different emission colors of these samples are caused by the quantum size effect [38]. The high-resolution TEM (HRTEM) images reveal that there is only one kind of well-resolved lattice fringe in these SiCDs with a lattice distance of 0.21 nm, which corresponds to the (100) in-plane lattice of graphene [39]. The powder X-ray diffraction (XRD) patterns of the four samples are characterized by a broad peak at about 21° with the interlayer spacing of 0.41 nm (Fig. S6), which is greater than that in the bulk graphite (0.32 nm), suggesting the presence of polymer chains on the graphene edge [40]. The increase in the diffraction intensity implies that the degree of graphitization is increasing from B-SiCDs to R-SiCDs, which is also corroborated by the Raman spectra. In Fig. 4, two peaks are observed at 1362 and 1,586 cm^{-1}, which are ascribed to the disordered or defective carbon (D band) and the well-organized graphitic carbon (G band) of the CDs, respectively [41]. The intensity ratio of I_D/I_G decreases from 0.94 to 0.83 for B-SiCDs to R-SiCDs, meaning a gradual increase in the size of sp^2-domains in these SiCDs, which agrees well with the above SEM, TEM, and XRD results.

The chemical compositions and functional groups of the four SiCDs are further investigated by Fourier transform infrared (FTIR) spectra and X-ray photoelectron spectroscopy (XPS). In Fig. 5, the FTIR results display several similar absorption peaks in the range of 500–4000 cm^{-1}, indicating that the four SiCDs have similar chemical compositions. To be specific, the absorption bands at 3526-3200 cm^{-1} are ascribed to the

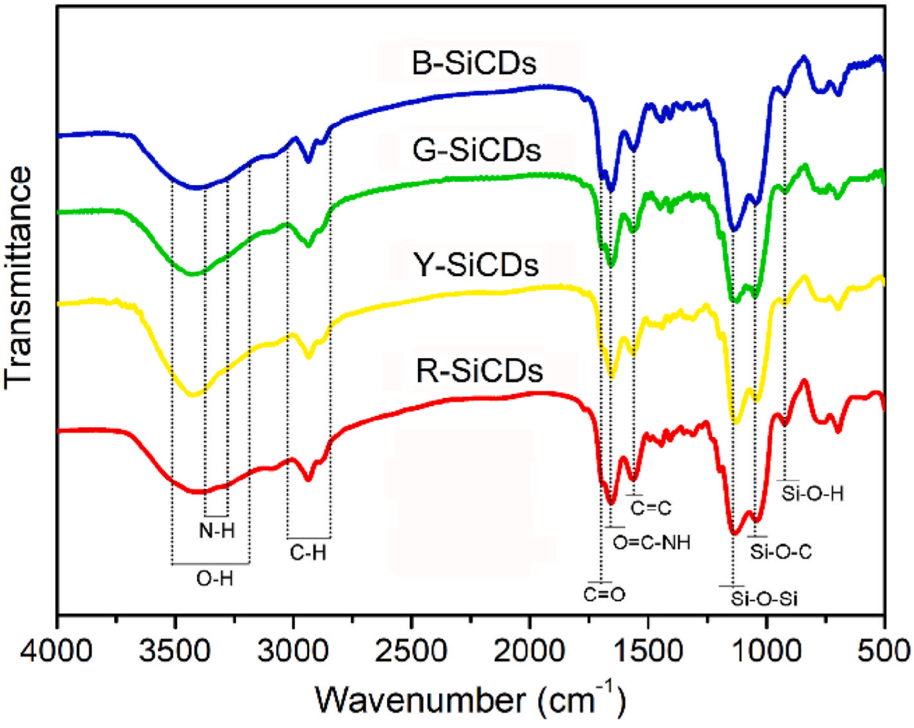

Fig. 5. FTIR spectra of the four selected SiCDs. (A colour version of this figure can be viewed online.)

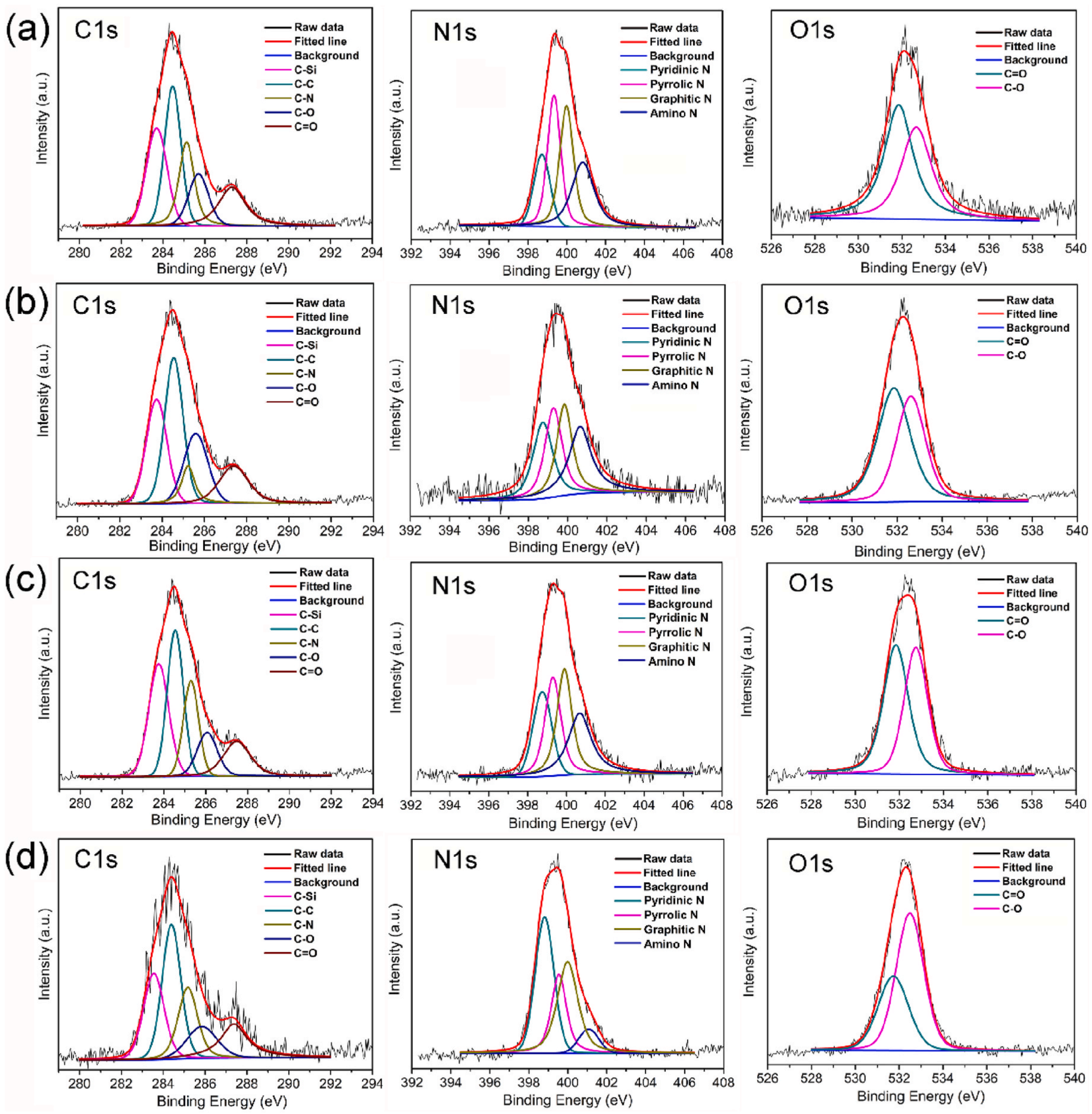

Fig. 6. High-resolution C 1s, N 1s, and O 1s XPS spectra of (a) B-SiCDs, (b) G-SiCDs, (c) Y-SiCDs, and (d) R-SiCDs, respectively. (A colour version of this figure can be viewed online.)

stretching vibration of –OH and –NH_2. The intense absorption peaks at 2984 cm^{-1}, 1603 cm^{-1}, and 1578 cm^{-1} correspond to the presence of C–H, –CONH, and C=C, respectively, which reveals that the APTES is linked to the surface of carbon cores through amide bonds [40]. The absorption peaks located at 1159 cm^{-1}, 1034 cm^{-1}, and 917 cm^{-1} belong to the signal of Si–O–Si, Si–O–C, and Si–O–H, respectively, suggesting the formation of a cross-linked “Si–O–Si” network structure on CD surfaces due to the hydrolysis and condensation of APTES (Fig. S7) [42,43]. Remarkably, the stretching vibration intensity of C=O bonds at 1698 cm^{-1} gradually decreases from B-SiCDs to R-SiCDs, indicating these SiCDs have an increased carbonization degree with their red-shifted PL emission. In Fig. S8, the full XPS spectra show four major peaks at 102, 284, 400, and 532 eV, signifying all samples have the same elemental composition comprising C, N, O, and Si [44]. In the high-resolution XPS spectra (Fig. 6), the C 1s band can be deconvoluted into five peaks corresponding to C–Si at 283.6 eV, C–C at 284.5 eV, C–N at 285.2 eV, C–O at 285.8 eV, and C=O at 287.4 eV. The N 1s band can be decomposed into four peaks at 398.6, 399.3, 400.1, and 400.9 eV for pyridinic N, pyrrolic N, graphitic N, and amino N, respectively [45]. The Si 2p band can be divided into three peaks at 101.1, 101.8, and 102.4 eV, representing Si–C, Si–N, and Si–O, respectively (Fig. S9) [20]. The O 1s spectra display two oxygen types of C=O at 531.8 eV and C–O at 532.7 eV. The relevant data in Tables S3–5 obtained by XPS results reveal two important observations. One is that the atomic ratio between oxygen and carbon decreases from 49.5% of the B-SiCDs to 35.47% of the R-SiCDs, implying an increasing degree of carbonization in these SiCDs, which is consistent with the FTIR results. The other is that the sp^2 carbon content increases from 30.56% to 33.75% as the graphitic N content increases from 25.62% to 28.86% for B-SiCDs to R-SiCDs, again proving that the size of the conjugated π-domain increases with the red shift of emission [46]. The above results indicate that the generated polymer chains and network structure on the surface of SiCDs can prevent the graphitized nuclei from π–π interactions and then achieve solid-state luminescence, and that the differences in carbon cores of these SiCDs are associated with their red-shifted PL emission from blue to red.

Taken together, it is clear that these SiCDs are N doped, coated with abundant polymer chains and network structure, and have a highly

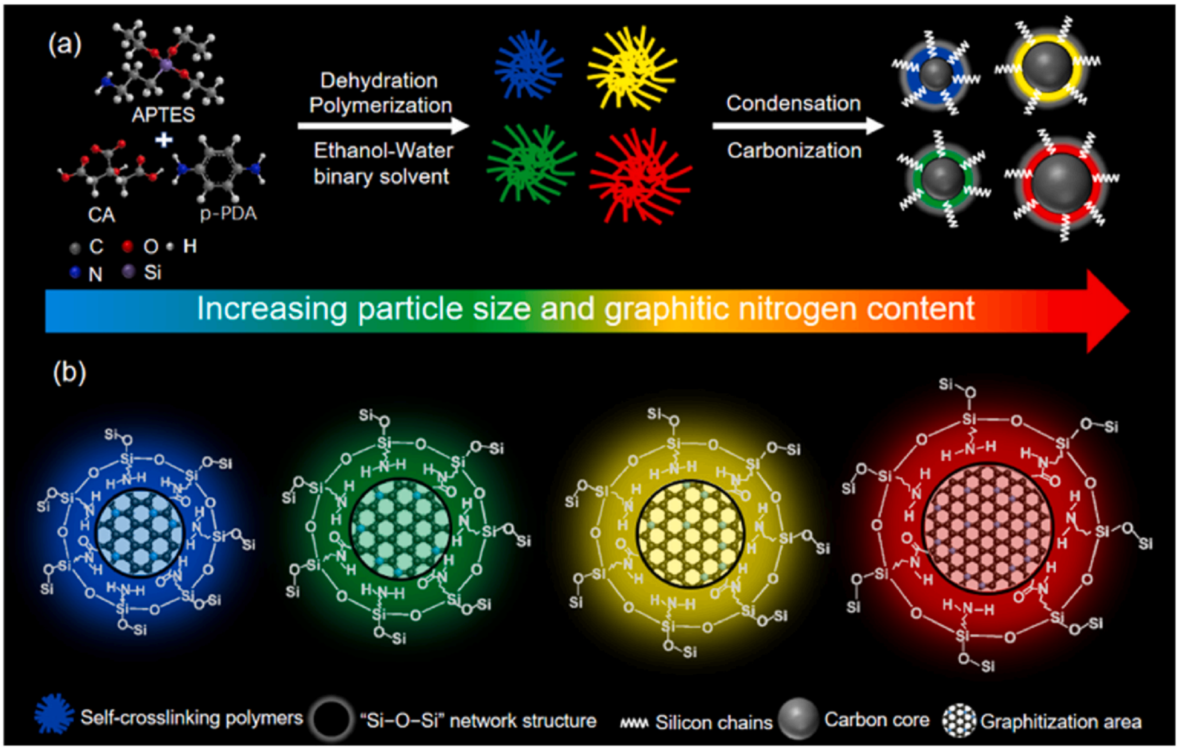

Scheme 1. Schematic illustration of the four selected SiCDs for their (a) formation mechanism and (b) PL mechanism.

graphitized core, yielding intense solid-state PL emission. Taking a step further, we deduce a possible growth process for these SiCDs, which is proposed in Scheme 1a. At the initial reaction stage, the carboxyl groups of CA react with the amine groups of both p-PDA and APTES to produce polymer aggregate nanoparticles through dehydration and condensation reaction [47–49]. Then, these self-crossing polymer nanoparticles are partially carbonized at elevated reaction temperatures and pressures, yielding CDs with a graphitized core embedded in the entangled organosilicon polymers via amide bonds [50,51]. In the meantime, the surface APTES also undergo hydrolysis and condensation reactions and form a "Si–O–Si" network structure to wrap the generated CDs. When the content of p-PDA added is increased, more benzene rings will be fused together to generate a large-sized rigid π-conjugated structure in carbon cores through dehydration and condensation reaction between CA and p-PDA. As a result, different-sized silane-functionalized CDs can be achieved by just changing the amount of p-PDA in the reaction system.

In order to further disclose the origins of multicolor emission of these SiCDs, the aggregation degree of CDs in the "Si–O–Si" network structure was further measured by thermogravimetric analysis (TGA). In Fig. S10, these SiCDs possess three decomposition stages. The initial weight loss before 150 °C results from the evaporation of physically adsorbed water [52]. The subsequent weight losses during 290–430 °C and 500–650 °C should correspond to the decomposition of organic species and oxidized sp^2 structures in the"Si–O–Si" matrix, respectively [43]. When the temperature exceeds 800 °C, the weight loss of these samples decreases slightly in the order of B-SiCDs, G-SiCDs, Y-SiCDs, and R-SiCDs, meaning nearly the same CD loading fraction in these SiCDs composites, which is different from previously reported CDs-based hybrid materials with multicolor emission [20,25]. Besides, the fluorescent characteristics of these SiCDs were investigated after etching their "Si–O–Si" network structure on surfaces with an alkaline solution ($pH = 13$). In Fig. S11, all the alkali-treated samples are shown to be self-quenched in solid state, again confirming that the polymer matrixes play a dominant role in reducing the AIQ effect. However, when they are dispersed in ethanol, these alkali-treated SiCDs exhibit a concentration-independent emission, with the fluorescent colors and PL peaks similar to those of the corresponding SiCDs powders (Figs. S12 and 13). These data clearly prove that the multicolor emissions of our SiCDs arise from their significant changes in structural components, rather than the aggregation-induced PL red-shift due to FRET or reabsorption [25]. It has been reported that both the larger π-electron system and the higher graphitic nitrogen content would create narrowed energy gaps between the highest occupied molecular orbital and the lowest unoccupied molecular orbital, consequently tuning the PL emission of CDs toward longer wavelength regions [33]. Based on these results and conclusions, it is concluded that the adjustment of emitting color of these solid SiCDs can be achieved by increasing both the sp^2-conjugated domain and graphitic N content in their carbon cores (Scheme 1b). Remarkably, due to the improved content of graphitic N, these SiCDs do not exhibit a significant downward trend in PL QYs with their PL red shift, which is contrary to other reported CDs with a surface-state emission [21,25]. This is because graphitic N not only can donate delocalized electrons to increase the probability of the radiative process but also can enhance the rigidity of aromatic domains to reduce the probability of nonradiative processes (*i.e.* molecular vibrations) [23,33]. As a result, these SiCDs maintain high solid-state PL QYs across the entire visible spectrum.

Benefiting from their full-color emission, high solid-state QYs, and high production yields, these SiCDs can be employed as color-converting layers to fabricate LEDs. Before this application, the fluorescent stability of these SiCDs powders at high temperatures or long-time storage under ambient conditions was first tested. All the results in Figs. S14 and 15 show that these SiCDs are quite stable without distinct PL fluctuation, which is important for their practical applicability in LEDs [40]. Four types of monochrome LEDs were obtained by coating 365 nm UV chips with thermal-curable silicone resin containing B-, G-, Y-, and R-SiCDs, respectively. In Fig. 7a–d, the obtained LEDs devices produce luminous blue, green, yellow, and red light with peaks at 439, 520, 565, to 628 nm, respectively (Fig. S16), and CIE coordinates of (0.22, 0.27), (0.30, 0.53), (0.44, 0.51), and (0.60, 0.31), respectively (Fig. S17). The broadband luminescent properties of these monochromatic LEDs inspire

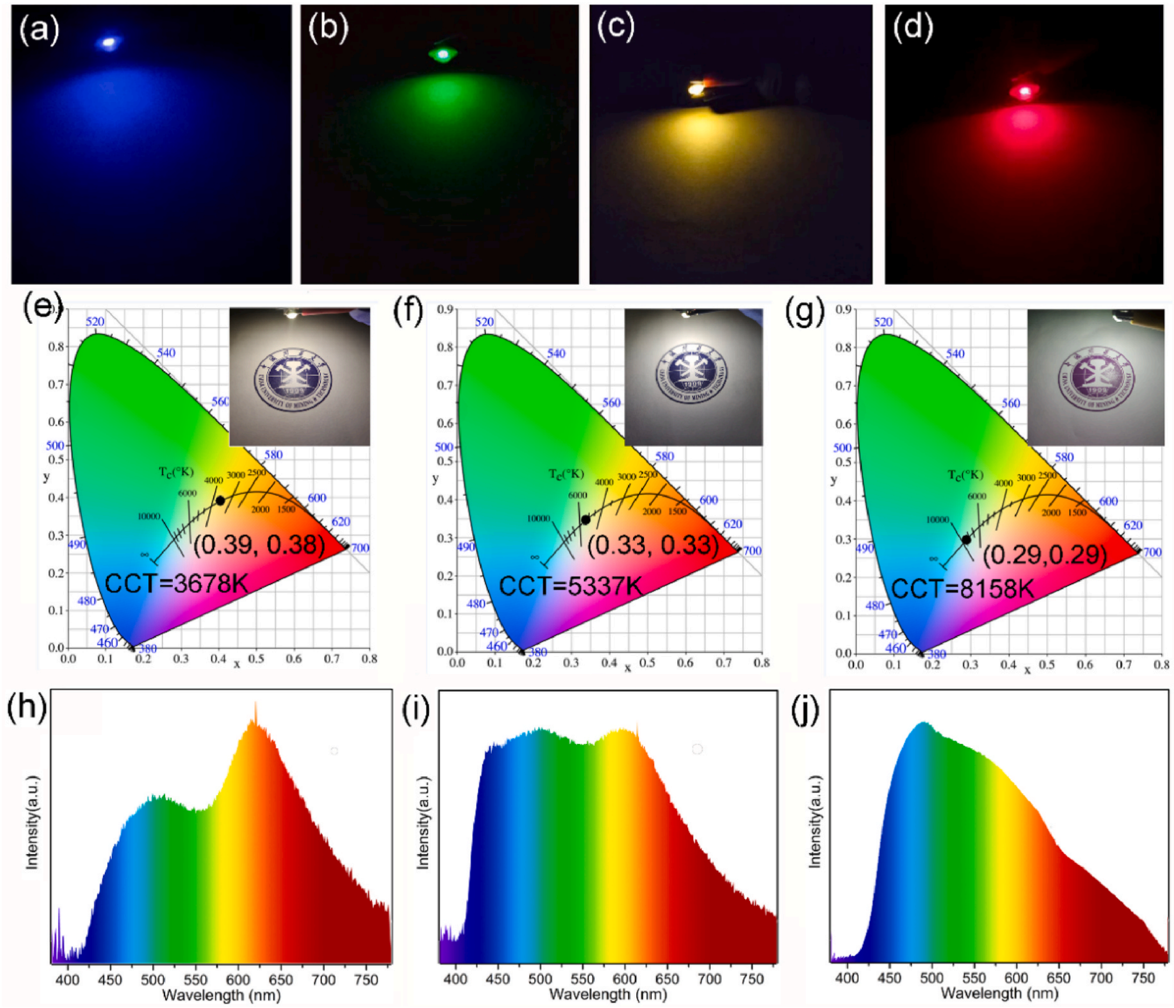

Fig. 7. Optical photographs of operating (a) B-, (b) G-, (c) Y-, and (d) R-SiCDs-based LEDs. (e and h) The CIE color coordinates and corresponding emission spectrum of the warm WLED (inset: optical photograph of the warm WLED). (f and i) The CIE color coordinates and corresponding emission spectrum of the standard WLED (inset: optical photograph of the standard WLED). (g and j) The CIE color coordinates and corresponding emission spectrum of the cool WLED (inset: optical photograph of the cool WLED). (A colour version of this figure can be viewed online.)

us to further construct WLEDs using B-, G-, and R-SiCDs. When the mass ratio of B-, G-, and R-silica/CDs is fixed at 0.6:1.0:1.3, a warm WLED is obtained with CCT of 3678 K, CIE coordinates of (0.39, 0.38), and CRI of 94 (Fig. 7e). The emitted bright warm white light is highly desired for indoor illuminates due to their comfortable ambient lighting [53]. When the mass ratio is changed to 0.9:1.3:1.2, a standard WLED with CIE coordinates of (0.33, 0.33) is achieved (Fig. 7f), which generates white light close to natural sunlight. The CCT (5337 K) and CRI (92) of the pure WLED perform better than those of most CD-based WLEDs [54–56]. Finally, a cool WLED is acquired with a mass ratio of 1.4:1.0:0.7. Their CCT, CIE coordinates, and CRI are 8158K, (0.29, 0.29), and 90, respectively (Fig. 7g). The emission spectra of the three types of WLEDs are shown in Fig. 7h–j and cover the entire visible light region from 380 to 780 nm. More importantly, after continuously operation over 96 h, the three types of WLEDs remain 90% of the initial PL intensity, suggesting their excellent photostabilities (Fig. S18). Wholly, these full-color SiCDs have great practical applications in solid-state lighting devices.

4. Conclusion

In summary, we have successfully achieved the large-scale synthesis of highly efficient full-color solid-state fluorescent SiCDs *via* the one-step microwave-assisted heating of the carefully selected precursors of CA, p-PDA, and APTES. The surface polymer chains and network structure can effectively prevent the π-π interaction between the graphitized cores, thus resisting the self-quenching of SiCDs in the aggregation state. Meanwhile, the emission colors of these SiCDs can be tuned from blue to red by adjusting the amount of p-PDA in the reaction system to control the size of sp^2-conjugated domains and the content of graphitic nitrogen in carbon cores. To our knowledge, this is the simplest way to acquire solid-state CDs with efficient full-color emission on a large scale. The resultant SiCDs are characterized by full-color emission, high yield, high solid-state QY, and good photostability, allowing us to fabricate full-color LEDs and multiple types of WLEDs with adjustable CCT from 3678 to 8158 K and high CRI of 90–94. This work provides a facile, controllable, and efficient route to produce CDs-based phosphors with excellent fluorescence properties and high production yields, giving CDs widespread potential in the practical application of lighting devices.

CRediT authorship contribution statement

Guangzhou Hu: Methodology, Formal analysis, Investigation, Writing – original draft, Data curation. **Yang Wang:** Investigation, Formal analysis, Data curation. **Shuang Zhang:** Formal analysis, Data curation. **Hui Ding:** Conceptualization, Investigation, Writing – review & editing, Resources, Project administration, Funding acquisition. **Ziyuan Zhou:** Investigation. **Jishi Wei:** Formal analysis. **Xuehua Li:**

Investigation. **Huanming Xiong:** Investigation, Supervision, Writing – review & editing.

Declaration of competing interest

The authors declare that they have no known competing financial interests or personal relationships that could have appeared to influence the work reported in this paper.

Acknowledgments

The authors acknowledge financial support from the National Natural Science Foundation of China (51803233, 22107045, 52004279 and 21975048), China Postdoctoral Science Foundation (2019M651999), and the Foundation for Basic and Applied Research of Guangdong Province (2019A1515110489).

Appendix A. Supplementary data

Supplementary data to this article can be found online at https://doi.org/10.1016/j.carbon.2022.11.048.

References

[1] H. Ding, X.X. Zhou, J.S. Wei, X.B. Li, B.T. Qin, X.B. Chen, H.M. Xiong, Carbon dots with red/near-infrared emissions and their intrinsic merits for biomedical applications, Carbon 167 (2020) 322–344.

[2] C. He, P. Xu, X. Zhang, W. Long, The synthetic strategies, photoluminescence mechanisms and promising applications of carbon dots: current state and future perspective, Carbon 186 (2022) 91–127.

[3] B. Wang, H. Cai, G.I.N. Waterhouse, X. Qu, B. Yang, S. Lu, Carbon dots in bioimaging, biosensing and therapeutics: a comprehensive review, Small Sci. 2 (6) (2022), 2200012.

[4] C. Kang, S. Tao, F. Yang, B. Yang, Aggregation and luminescence in carbonized polymer dots, Aggregate 3 (2) (2022) e169.

[5] H. Wu, S. Lu, B. Yang, Carbon-dot-enhanced electrocatalytic hydrogen evolution, Acc. Mater. Res. 3 (3) (2022) 319–330.

[6] Y. Ru, L. Sui, H. Song, X. Liu, Z. Tang, S.Q. Zang, B. Yang, S. Lu, Rational design of multicolor-emitting chiral carbonized polymer dots for full-color and white circularly polarized luminescence, Angew. Chem., Int. Ed. 60 (25) (2021) 14091–14099.

[7] B. Wang, J. Yu, L. Sui, S. Zhu, Z. Tang, B. Yang, S. Lu, Rational design of multi-color-emissive carbon dots in a single reaction system by hydrothermal, Adv. Sci. 8 (1) (2020), 2001453.

[8] J. Liu, R. Li, B. Yang, Carbon dots: a new type of carbon-based nanomaterial with wide applications, ACS Cent. Sci. 6 (12) (2020) 2179–2195.

[9] B. Zhi, X. Yao, M. Wu, A. Mensch, Y. Cui, J. Deng, J.J. Duchimaza-Heredia, K. J. Trerayapiwat, T. Niehaus, Y. Nishimoto, B.P. Frank, Y. Zhang, R.E. Lewis, E. A. Kappel, R.J. Hamers, H.D. Fairbrother, G. Orr, C.J. Murphy, Q. Cui, C.L. Haynes, Multicolor polymeric carbon dots: synthesis, separation and polyamide-supported molecular fluorescence, Chem. Sci. 12 (7) (2020) 2441–2455.

[10] J. Wang, Y. Yang, X. Liu, Solid-state fluorescent carbon dots: quenching resistance strategies, high quantum efficiency control, multicolor tuning, and applications, Mater. Adv. 1 (9) (2020) 3122–3142.

[11] T. Meng, Z. Wang, T. Yuan, X. Li, Y. Li, Y. Zhang, L. Fan, Gram-scale synthesis of highly efficient rare-earth-element-free red/green/blue solid-state bandgap fluorescent carbon quantum rings for white light-emitting diodes, Angew. Chem., Int. Ed. 60 (30) (2021) 16343–16348.

[12] K. Jiang, Y.H. Wang, Z.J. Li, H.W. Lin, Afterglow of carbon dots: mechanism, strategy and applications, Mater. Chem. Front. 4 (2) (2020) 386–399.

[13] D. Zhou, P. Jing, Y. Wang, Y. Zhai, D. Li, Y. Xiong, A.V. Baranov, S. Qu, A. L. Rogach, Carbon dots produced via space-confined vacuum heating: maintaining efficient luminescence in both dispersed and aggregated states, Nanoscale Horiz 4 (2) (2019) 388–395.

[14] X. Dong, Y. Wang, R. Guan, J. Ren, Z. Xie, Silane-functionalized carbon dots and their polymerized hybrids: from optoelectronics to biotherapy, Small 17 (50) (2021), 2105273.

[15] D. Zhou, Y. Zhai, S. Qu, D. Li, P. Jing, W. Ji, D. Shen, A.L. Rogach, Electrostatic assembly guided synthesis of highly luminescent carbon-nanodots@BaSO4 hybrid phosphors with improved stability, Small 13 (6) (2017), 1602055.

[16] J. Shao, S. Zhu, H. Liu, Y. Song, S. Tao, B. Yang, Full-color emission polymer carbon dots with quench-resistant solid-state fluorescence, Adv. Sci. 4 (12) (2017), 1700395.

[17] C.-L. Shen, J.-H. Zang, Q. Lou, L.-X. Su, Z. Li, Z.-Y. Liu, L. Dong, C.-X. Shan, In-situ embedding of carbon dots in a trisodium citrate crystal matrix for tunable solid-state fluorescence, Carbon 136 (2018) 359–368.

[18] A. Xu, G. Wang, Y. Li, H. Dong, S. Yang, P. He, G. Ding, Carbon-based quantum dots with solid-state photoluminescent: mechanism, implementation, and application, Small 16 (48) (2020), 2004621.

[19] L. Meng, E.V. Ushakova, Z. Zhou, E. Liu, D. Li, D. Zhou, Z. Tan, S. Qu, A.L. Rogach, Microwave-assisted in situ large scale synthesis of a carbon dots@g-C3N4 composite phosphor for white light-emitting devices, Mater. Chem. Front. 4 (2) (2020) 517–523.

[20] Y. Zhan, B. Shang, M. Chen, L. Wu, One-step synthesis of silica-coated carbon dots with controllable solid-state fluorescence for white light-emitting diodes, Small 15 (24) (2019), e1901161.

[21] H. Song, X. Liu, B. Wang, Z. Tang, S. Lu, High production-yield solid-state carbon dots with tunable photoluminescence for white/multi-color light-emitting diodes, Sci. Bull. 64 (23) (2019) 1788–1794.

[22] X.Q. Zhang, H.Y. Yang, Z.J. Wan, T. Su, X.J. Zhang, J.L. Zhuang, B.F. Lei, Y.L. Liu, C.F. Hu, Self-quenching-resistant red emissive carbon dots with high stability for warm white light-emitting diodes with a high color rendering index, Adv. Opt. Mater. 8 (15) (2020), 2000251.

[23] J.L. Wang, Q. Li, J.X. Zheng, Y.Z. Yang, X.G. Liu, B.S. Xu, N, B-codoping induces high-efficiency solid-state fluorescence and dual emission of yellow/orange carbon dots, ACS Sustainable Chem. Eng. 9 (5) (2021) 2224–2236.

[24] B.E. Kwak, H.J. Yoo, D. Kim, Quenching-resistant polymer carbon dot preserving emission color consistency in solid-state, Adv. Opt. Mater. 7 (23) (2019), 1900932.

[25] J. Wang, J. Zheng, Y. Yang, X. Liu, J. Qiu, Y. Tian, Tunable full-color solid-state fluorescent carbon dots for light emitting diodes, Carbon 190 (2022) 22–31.

[26] F. Yan, C. Yi, J. Sun, Y. Zang, Y. Wang, M. Xu, J. Xu, Self-quenching-resistant solid-state carbon dots for mechanism and applications, Mikrochim. Acta 188 (12) (2021) 412.

[27] H. Yang, Y. Liu, Z. Guo, B. Lei, J. Zhuang, X. Zhang, Z. Liu, C. Hu, Hydrophobic carbon dots with blue dispersed emission and red aggregation-induced emission, Nat. Commun. 10 (1) (2019) 1789.

[28] Y. Chen, M. Zheng, Y. Xiao, H. Dong, H. Zhang, J. Zhuang, H. Hu, B. Lei, Y. Liu, A self-quenching-resistant carbon-dot powder with tunable solid-state fluorescence and construction of dual-fluorescence morphologies for white light-emission, Adv. Mater. 28 (2) (2016) 312–318.

[29] J.Y. Zhu, X. Bai, X. Chen, H. Shao, Y. Zhai, G.C. Pan, H.Z. Zhang, E.V. Ushakova, Y. Zhang, H.W. Song, A.L. Rogach, Spectrally tunable solid state fluorescence and room-temperature phosphorescence of carbon dots synthesized via seeded growth method, Adv. Opt. Mater. 7 (9) (2019), 1801599.

[30] Y. Zhao, C. Ou, J. Yu, Y. Zhang, H. Song, Y. Zhai, Z. Tang, S. Lu, Facile synthesis of water-stable multicolor carbonized polymer dots from a single unconjugated glucose for engineering white light-emitting diodes with a high color rendering index, ACS Appl. Mater. Interfaces 13 (25) (2021) 30098–30105.

[31] F. Liu, S. Xu, P. Xia, H. Yang, Z. Qian, Y. Jiang, Z. Wang, D. Ban, C. Wang, Anhydride-terminated solid-state carbon dots with bright orange emission induced by weak excitonic electronic coupling, ACS Appl. Mater. Interfaces 14 (4) (2022) 5762–5774.

[32] L. Cao, M. Zan, F. Chen, X. Kou, Y. Liu, P. Wang, Q. Mei, Z. Hou, W.-F. Dong, L. Li, Formation mechanism of carbon dots: from chemical structures to fluorescent behaviors, Carbon 194 (2022) 42–51.

[33] H. Ding, X.X. Zhou, Z.H. Zhang, Y.P. Zhao, J.S. Wei, H.M. Xiong, Large scale synthesis of full-color emissive carbon dots from a single carbon source by a solvent-free method, Nano Res. 15 (4) (2022) 3548–3555.

[34] Y. Zheng, K. Arkin, J. Hao, S. Zhang, W. Guan, L. Wang, Y. Guo, Q. Shang, Multicolor carbon dots prepared by single-factor control of graphitization and surface oxidation for high-quality white light-emitting diodes, Adv. Opt. Mater. 9 (19) (2021), 2100688.

[35] H. Ding, J.S. Wei, P. Zhang, Z.Y. Zhou, Q.Y. Gao, H.M. Xiong, Solvent-Controlled synthesis of highly luminescent carbon dots with a wide color gamut and narrowed emission peak widths, Small 14 (22) (2018), e1800612.

[36] S. Khan, A. Gupta, N. Verma, C. Nandi, Time-resolved emission reveals ensemble of emissive states as the origin of multicolor fluorescence in carbon dots, Nano Lett. 15 (12) (2015) 8300–8305.

[37] X. Xu, L. Mo, W. Li, Y. Li, B. Lei, X. Zhang, J. Zhuang, C. Hu, Y. Liu, Red, green and blue aggregation-induced emissive carbon dots, Chin. Chem. Lett. 32 (12) (2021) 3927–3930.

[38] B. Zhao, H. Ma, M. Zheng, K. Xu, C. Zou, S. Qu, Z.a. Tan, Narrow-bandwidth emissive carbon dots: a rising star in the fluorescent material family, Carbon Energy 4 (1) (2022) 88–114.

[39] L. Wang, W. Li, L. Yin, Y. Liu, H. Guo, J. Lai, Y. Han, G. Li, M. Li, J. Zhang, R. Vajtai, P.M. Ajayan, M. Wu, Full-color fluorescent carbon quantum dots, Sci. Adv. 6 (40) (2020), eabb6772.

[40] Y. Wu, Y. Zhan, W. Xin, W. Cao, J. Li, M. Chen, X. Jiang, J. Wang, Z. Sun, Highly emissive carbon dots/organosilicon composites for efficient and stable luminescent solar concentrators, ACS Appl. Energy Mater. 5 (2) (2022) 1781–1792.

[41] B. Lyu, H.-J. Li, F. Xue, L. Sai, B. Gui, D. Qian, X. Wang, J. Yang, Facile, gram-scale and eco-friendly synthesis of multi-color graphene quantum dots by thermal-driven advanced oxidation process, Chem. Eng. J. 388 (2020), 124285.

[42] F. Yan, H. Zhang, J. Xu, Y. Wu, Y. Zang, J. Sun, Color emission carbon dots with quench-ResixAstant solid-state fluorescence for light-emitting diodes, ACS Sustain. Chem. Eng. 9 (10) (2021) 3901–3908.

[43] J. Wu, W. Xin, Y. Wu, Y. Zhan, J. Li, J. Wang, S. Huang, X. Wang, Solid-state photoluminescent silicone-carbon dots/dendrimer composites for highly efficient luminescent solar concentrators, Chem. Eng. J. 422 (2021), 130158.

[44] J. He, Y. He, Y. Chen, B. Lei, J. Zhuang, Y. Xiao, Y. Liang, M. Zheng, H. Zhang, Y. Liu, Solid-state carbon dots with red fluorescence and efficient construction of dual-fluorescence morphologies, Small 13 (26) (2017), 1700075.

[45] H. Ding, X. Zhou, Z. Zhang, K. Xia, Y. Zhao, Solvent-free and high-yielding synthesis of highly efficient red-emitting carbon dots and their application in white light devices, Chem. J. Chin. Univ. 42 (6) (2021) 2080–2084.

[46] S. Wei, X. Yin, H. Li, X. Du, L. Zhang, Q. Yang, R. Yang, Multi-color fluorescent carbon dots: graphitized sp(2) conjugated domains and surface state energy level Co-modulate band gap rather than size effects, Chem. Eur J. 26 (36) (2020) 8129–8136.
[47] D. Qu, Z. Sun, The formation mechanism and fluorophores of carbon dots synthesized via a bottom-up route, Mater. Chem. Front. 4 (2) (2020) 400–420.
[48] B. Wang, S. Lu, The light of carbon dots: from mechanism to applications, Matter 5 (1) (2022) 110–149.
[49] Y. Shi, H. Xu, T. Yuan, T. Meng, H. Wu, J. Chang, H. Wang, X. Song, Y. Li, X. Li, Y. Zhang, W. Xie, L. Fan, Carbon dots: an innovative luminescent nanomaterial, Aggregate 3 (3) (2021) e108.
[50] L. Vallan, H. Imahori, Citric acid-based carbon dots and their application in energy conversion, ACS Appl. Electron. Mater. 4 (9) (2022) 4231–4257.
[51] L. Ai, Y. Yang, B. Wang, J. Chang, Z. Tang, B. Yang, S. Lu, Insights into photoluminescence mechanisms of carbon dots: advances and perspectives, Sci. Bull. 66 (8) (2021) 839–856.
[52] R. Dai, X. Chen, N. Ouyang, Y. Hu, A pH-controlled synthetic route to violet, green, and orange fluorescent carbon dots for multicolor light-emitting diodes, Chem. Eng. J. 431 (2022), 134172.
[53] Z. Wang, F. Yuan, X. Li, Y. Li, H. Zhong, L. Fan, S. Yang, 53% efficient red emissive carbon quantum dots for high color rendering and stable warm white-light-emitting diodes, Adv. Mater. 29 (37) (2017), 1702910.
[54] Y. Zhang, P. Zhuo, H. Yin, Y. Fan, J. Zhang, X. Liu, Z. Chen, Solid-state fluorescent carbon dots with aggregation-induced yellow emission for white light-emitting diodes with high luminous efficiencies, ACS Appl. Mater. Interfaces 11 (27) (2019) 24395–24403.
[55] W. Cai, T. Zhang, M. Xu, M. Zhang, Y. Guo, L. Zhang, J. Street, W.-J. Ong, Q. Xu, Full color carbon dots through surface engineering for constructing white light-emitting diodes, J. Mater. Chem. C 7 (8) (2019) 2212–2218.
[56] P. He, Y. Shi, T. Meng, T. Yuan, Y. Li, X. Li, Y. Zhang, L. Fan, S. Yang, Recent advances in white light-emitting diodes of carbon quantum dots, Nanoscale 12 (8) (2020) 4826–4832.